

# Dual-Frequency Plasma Enhanced Chemical Vapor Deposition of Diamond-Like Carbon Thin Films

R. JAMSHIDI<sup>a</sup>, S.I. HOSSEINI<sup>b,\*</sup> AND Y. AHMADIZADEH<sup>c</sup>

<sup>a</sup>Islamic Azad University, South Tehran Branch, Tehran, Iran

<sup>b</sup>Laser and Plasma Research Institute, Shahid Beheshti University, G.C., Evin, Tehran, Iran

<sup>c</sup>Faculty of Science, University of Aeronautical Science and Technology, Tehran, Iran

(Received August 21, 2011; in final form March 18, 2012)

Dual-frequency plasma enhanced chemical vapor deposition was used to grow diamond-like carbon thin films from CH<sub>4</sub>, H<sub>2</sub> gas mixture. The effects of radio frequency, microwave power, and gas ratio were investigated. Various species have been identified in the CH<sub>4</sub>-H<sub>2</sub> plasma using optical emission spectroscopy and their effects on film properties have been studied. Increasing the RF power to 400 W, the variation trend of refractive index and CH, C<sub>2</sub> intensity ratios change beyond the 300 W, but the growth rate shows the continuous increasing character from 6 to 11.6 nm/min. Increasing the hydrogen content in the system, the intensity ratio of CH, C<sub>2</sub>, CH<sup>+</sup> and growth rate show decreasing tendency and the refractive index rises from 1.98 to 2.63. Adding MW produced plasma to the system grows the refractive index to 2.88 and growth rate to 10.8 nm/min. The water contact angle rises from 58.95° to 73.74° as the RF power increases to 300 W but begins to reduce until 400 W. In addition, the contact angle shows a growing tendency by increasing the hydrogen flow to the chamber. In addition, the structures of the films were investigated by the Raman spectroscopy.

PACS: 81.15.Gh

## 1. Introduction

Diamond-like carbon (DLC) is a name which is often applied to various amorphous carbon materials which have similar properties to that of diamond. DLC is a metastable material which was synthesized for the first time in 1971 by Aisenberg and Chabot with ion beam method [1]. DLC films show, to some extent, diamond characteristics such as high mechanical hardness [2], low friction coefficient, chemical inertness and resistance [3], low thermal expansion and transparency in IR section of the electromagnetic spectrum [4]. These features of DLC films are connected to the film structure. The structure of DLC film is a mixture of some graphitic  $sp^2$  and aliphatic  $sp^3$  bonding and the fraction ratio of them ( $sp^3/sp^2$ ) strongly ascertains the physical properties of it. In general, although the mechanical and chemical characteristics are governed by amount of the  $sp^3$  bonding, electronic and optical properties are associated to fraction of the  $sp^2$  bonding [5, 6]. Therefore, it is essential to have precise control on the fraction ratio to deposit a favorite layer relevance to the applications.

Researchers have reported several methods for coating of DLC films such as laser-assisted evaporation [7],

plasma enhanced chemical vapor deposition (PECVD) using radio frequency (RF) [8], filtered cathodic vacuum arc [9], electron cyclotron resonance [10], RF-assisted microwave [11], and plasma beam source [12]. In all these methods DLC films grow under ion bombardment and the energy of the incoming ion determine the  $sp^3/sp^2$  ratio.

Among these methods RF-assisted microwave plasma is the best, since the coating happens at low temperature with good step coverage by simple controlling on reaction parameters. The most important feature of this method is the ability of fine-tuning on the measure of density and energy of impinging ions, independently.

In this work, we investigate the effects of RF and MW power and feed gas ratio on the refractive index, roughness and growth rate. In addition, the produced ions, radicals and active species were studied by optical emission spectroscopy (OES).

## 2. Experiment

The experimental setup is shown in Fig. 1. The reaction chamber comprises two main sections, the MW and RF parts. The MW section consists of a quartz discharge tube with internal diameter of 32 mm and length of 600 mm. The waves are fed to the discharge tube via waveguide equipped with an impedance matching

\* corresponding author; e-mail: y.ahmadizadeh@gmail.com

network, a circulator and a field applicator. The surface waves were produced by a 300 W (Sairem GMP 03 KED) power generator and started propagating along the plasma column and sustained it when the plasma has been produced in the tube. The initial breakdown takes place in the discharge tube in the field applicator.

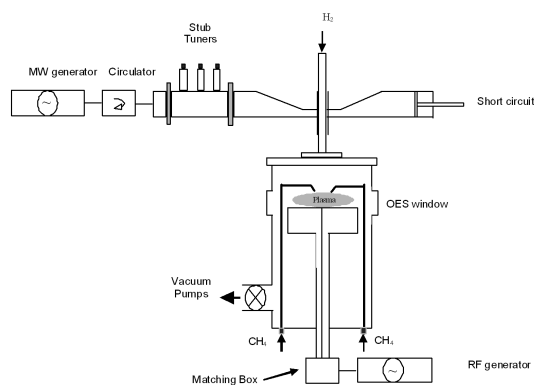


Fig. 1. Schematic of the dual-mode experimental set up.

RF section consists of the 34 MHz and 2.5 kW RF generator for producing the methane plasma. The ground electrode was gas injectors which was made up of 38 pipes with diameter of 270 mm and was placed 30 mm away from the powered electrode which was 150 mm in diameter. The substrates were mounted on the powered electrode, therefore it was equipped with water-cooling and electrical heating to control the temperature of the substrate during the process.

The substrates used throughout the experiments are 1 mm thick pieces of glass. Before putting the substrates in the chamber, they should be cleaned in the ultrasonic bath with acetone. The base pressure was  $10^{-3}$  mTorr and hydrogen is injected into the quartz tube through top of the chamber, reaching the MW section with 0, 60, 120 and 180 sccm flow rate which was being controlled by mass flow controller (UNIT instruments Co. UFC-1000HP). The 38 pipes injectors carry methane to the RF part of the system at a constant flow rate of 30 sccm. The effects of gas ratio  $R$  ( $H_2/CH_4$ ) and RF and MW power on the properties of 30 min deposited films have been investigated. Optical absorption and transmission spectrum was obtained by spectrometer (model Ocean Optics — USB2000). The thickness of the films was measured by surface profilometer Dektak 8000. Surface morphology of the films was characterized by Nanosurf easyscan 2 atomic force microscope (AFM) which can work in ambient air and the root mean square (rms) of surface roughness was derived from AFM data. Also optical emission spectra were recorded by Echelle spectrometer on ICCD to study the produced ions, radicals and excited species in the plasma. The structures of the films were investigated by the Raman spectra obtained from Alpha Thermo Nicolet Dispersive Raman Spectrometer (532 nm).

### 3. Results and discussions

Figure 2a, b shows the variation of the refractive index (at  $\lambda = 632.8$  nm) versus RF power (at  $R = 6$ ) and gas ratio (at  $W = 300$  W). The index of refraction was calculated through the Kramers–Kronig relations, using measured absorption and transmission spectra of DLC films [13]. In this method the Kramers–Kronig relations express the connection between the real and imaginary parts of dielectric function  $\epsilon$ , which is discussed and reviewed in detail at [14, 15]. As can be seen from Fig. 2a, the refractive index grows to 2.63 by increasing the RF power to 300 W, then decreases to 2.55 as the power increases to 400 W. Figure 2b shows the increasing tendency of the refractive index from 1.98 at  $R = 0$  to 2.63 at  $R = 6$ . In general, the hydrogen content and density of the film govern the index of refraction [16–18]. Increasing the RF power increases the density of active species and energy of incoming ions to the surface of the film which leads to growing the density of the film and increases the refractive index. The excessive energy of incident ions after 300 W of RF power, graphitizes the film structure and decreases the refractive index [19]. Having more hydrogen atoms in the deposition process abstracts more hydrogen bonds from the film front by formation of  $H_2$  molecules and creates many dangling bonds. Since carbon-containing ions have enough energy at 300 W of RF power, they can replace the abstracted hydrogen atom and bond to the surface of the film. This replacement grows the density of the film and one can see the increasing tendency of the refractive index with increasing the hydrogen fraction in the reactions. The hydrogen abstraction enhances by adding MW produced plasma to the system. Because MW produces denser plasma than that of RF [20], the concentration of hydrogen atoms augmented as the MW power increases. Therefore, the refractive index grows to 2.88 at 300 W of MW power.

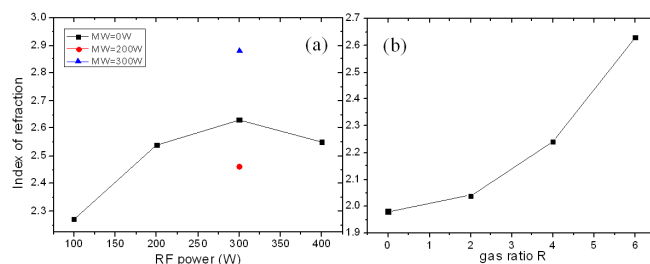


Fig. 2. Variation of refractive index versus (a) RF and MW power, (b) gas ratio.

Figure 3a, b illustrates the measured surface roughness of the films. The rms roughnesses of the films were measured by AFM. As can be seen from Fig. 3a initially, the rms roughness becomes lower as the RF power increases, then begins to grow with more RF and MW powers. The initial drop in surface roughness may be due to substantial contamination remain on the surface of the substrate at low RF power which gently becomes sputtered by in-

creasing the power to 200 W. As the energy of incoming ions increases by increasing the RF power, the sputtering of the surface of the film front enhances and the rms roughness grows to 0.9 nm. Since hydrogen atoms preferentially etch  $sp^2$  rich region probably formed on the surface of the film (Fig. 3b), the surface roughness shows an inverse trend and decreases continuously with increasing the hydrogen content [21, 22].

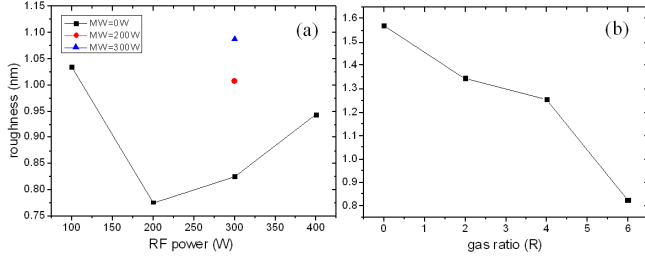


Fig. 3. Surface roughness of the films as a function of (a) RF and MW power, (b) gas ratio.

The growth rates of the films are demonstrated in Fig. 4a, b. The growth rate increases by raising the RF and MW power and decreases as the gas ratio increases. Generally, physical and chemical processes regulate the growth rate. Two key physical plasma parameters are the flux and energy of incident ions. When RF power grows, electrons oscillate with more energy that leads to more inelastic impact ionization and dissociation occurrence. Therefore, the density of active species and ions grows which increases the growth rate. Introducing the MW produced plasma to the system, the density of the plasma soars and the growth rate increases from 10 nm/min to 10.8 nm/min. In contrast, the growth rate goes down by increasing the gas ratio. Increasing the hydrogen fraction raises the sputtering rate of  $sp^2$  rich region that lowers the growth rate from 18.2 nm/min to 10 nm/min at 0 and 180 sccm of hydrogen, respectively.

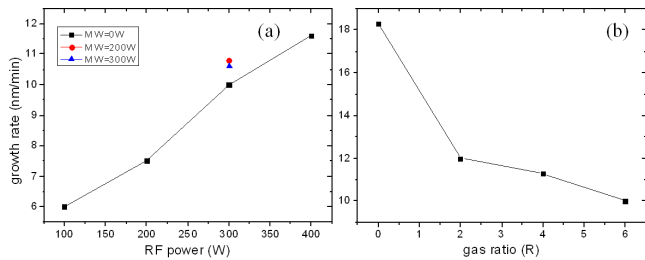


Fig. 4. Variation of growth rate versus (a) RF and MW power, (b) gas ratio.

OES is one of efficient and nondestructive methods to diagnose the plasma and identify the chemical and active species in the process. With this method, the variation of relative intensities of emission lines can be correlated with the obtained properties of deposited DLC films. Figure 5 shows some typical emission spectra of

the  $CH_4-H_2$  plasma in different conditions. The results reveal that the gas mixture decomposed to various hydrocarbon species such as CH (431.1 nm), CH (387.1 nm),  $CH^+$  (417.1 nm),  $C_2$  (516.3 nm) and hydrogen atoms.

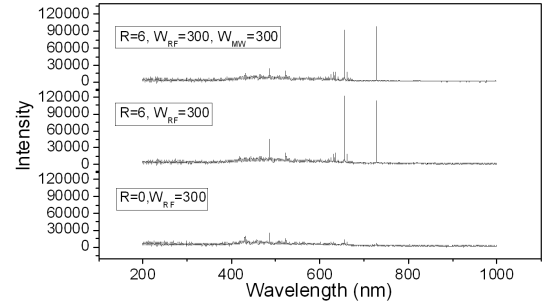


Fig. 5. Typical optical emission spectra at different conditions.

The electrical transitions which were observed in the plasma emission spectra are listed in Table I.

TABLE I

Emission species in the  $CH_4-H_2$  plasma during DLC growth.

Chemical species	$\lambda$ [nm]	Electronic transitions
$H_\alpha$ (Balmer)	656.2	$2p^2P^0-3d^2D$
$H_\beta$ (Balmer)	486.1	$2p^2P^0-4d^2D$
$H^+$ (Paschen)	820	$n = \infty \rightarrow n = 3$
CH	430.9	$A^2\Delta-X^2\Pi$
CH	387.5	$B^2\Sigma-X^2\Pi$
$CH^+$	417.1	$A^1\Pi-X^1\Pi$
$C_2$ (Swan)	516.3	$d^3\Pi_u-a^3\Pi_u$

Figure 6a reveals the intensity ratios of CH,  $CH^+$ ,  $C_2$  decrease and the intensity of  $H_\alpha$  increases as the hydrogen content rises in the process chamber. As mentioned before saturating the film front with the H atoms stabilizes the carbon  $sp^3$  bonding and makes carbon atoms stay in  $sp^3$  hybridization condition in the diamond metastable region [23]. In addition, H atoms etch  $sp^2$  rich region and prevent the nucleation and growth of graphite structures. Another important point is that the presence of CH radicals in the plasma medium is responsible for the growth rate and helps the formation of amorphous carbon and reduces the  $sp^3$  content in the film.

As can be seen from Fig. 6a, the increase of hydrogen content decreases the CH intensity ratio, favors the formation of the  $sp^3$  diamond structure. These results of optical emission spectroscopy are in complete agreement with the increasing and decreasing tendency of refractive index and growth rate of the films (Figs. 2, 4), respectively. A similar trend is observed in intensity ratios of species with increase of the RF power up to 300 W (Fig. 6b). However, the intensity ratio of CH and  $C_2$  increases as the RF power grows to 400 W. These results

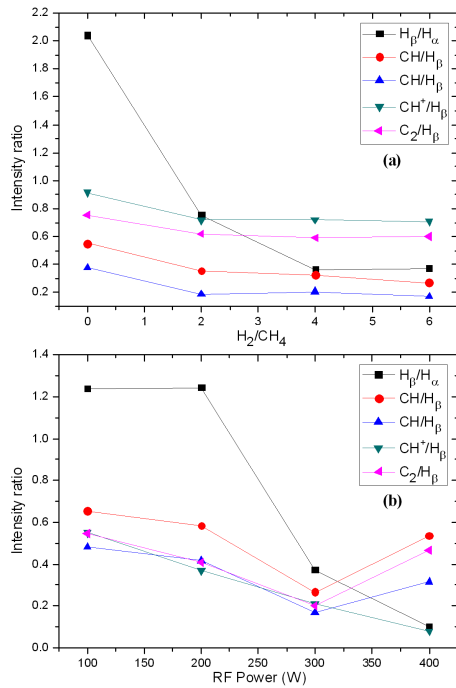


Fig. 6. Variation of OES intensity ratio of excited species: (a) different gas ratio, (b) various RF power.

also confirm the variation of refractive index that rises to 2.63 at 300 W of RF power and then drops to 2.55 at 400 W.

In spite of decreasing tendency of CH intensity ratios until 300 W, the growth rate continuously raised to 10 nm/min. Increase of the RF power leads to production of more active plasma that contains some other carbonaceous species like as C<sub>x</sub> and CH<sub>y</sub> which contribute in deposition process [24]. Hence, the growth rate rises up as the RF power increases that demonstrates that the CH radicals are not the only species who have the main role in deposition process. Increase of the RF power above 300 W changes the chemical compositions which leads to formation of *sp*<sup>2</sup> structure.

Figure 7 shows a growing trend of intensity ratios of species with introducing the MW plasma to the system. This is because of stronger dissociation occurrences in the MW plasma due to more energetic electrons generated in MW frequency [20]. This efficient ionization grows the ion intensities e.g. CH<sup>+</sup> and H<sup>+</sup> which leads to increase of the growth rate with respect to single RF mode.

Figure 8 shows the spherical forms of deionized water sessile drop on the deposited DLC films with different gas ratio (*R*) and RF power. Mainly the surface roughness and surface chemistry are two determinant parameters that govern the contact angle. Generally, the contact angle decreases as the surface roughness increases, especially for the angles lower than 90° [25, 26]. Moreover, the DLC films show hydrophobic nature because of its CH<sub>x</sub> *sp*<sup>3</sup> bonding which arise from surface chemistry [25, 27, 28]. The variation of water contact angle

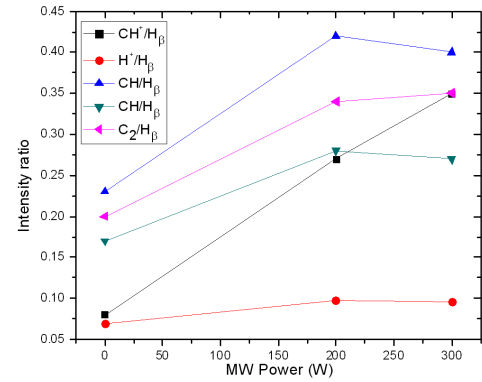


Fig. 7. Variation of OES intensity ratio of excited species at different MW power.

with RF power is shown in Fig. 9a. The contact angle rises from 58.95° to 73.74° as the RF power increases to 300 W then the contact angle gradually reduces to 68.32° with increasing the RF power to 400 W. This reduction in contact angle after 300 W is attributed to the changes of surface chemistry in which the CH<sub>x</sub> *sp*<sup>3</sup> bonding transform to CH *sp*<sup>2</sup> bonding due to higher energy of impinging ions to the surface. This is completely in agreement with OES data. As depicted in Fig. 9b, the contact angle continuously increases from 66.77° to 73.74° with the growing of H<sub>2</sub>/CH<sub>4</sub> ratio. This rising trend in contact angle is due to the decreasing tendency of surface roughness owed to etching of *sp*<sup>2</sup> rich region by hydrogen atoms.

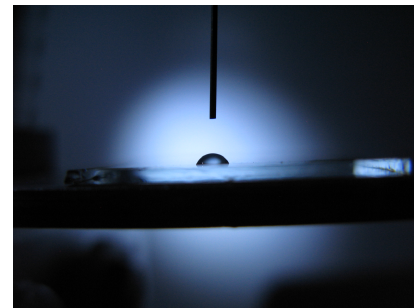


Fig. 8. A deionized water sessile drop on the DLC film surface.

Figure 10 shows the Raman spectra of deposited DLC films. The Raman spectrum of diamond-like carbon films has two broad bands, centered at 1540 cm<sup>-1</sup> and 1360 cm<sup>-1</sup> known as *G* and *D* peaks, respectively. The intensity and position of *G* and *D* peaks were obtained by fitting two Gaussian distributions to the Raman spectra and the results were summarized in Table II. The *sp*<sup>3</sup> fraction of the film can be estimated from the *G* peak position and *G*-*D* peaks intensity ratio (*I*<sub>*D*</sub>/*I*<sub>*G*</sub>). The *sp*<sup>3</sup> fraction of the films increases as the intensity ratio (*I*<sub>*D*</sub>/*I*<sub>*G*</sub>) decreases and the *G* peak shifts toward lower wave numbers [29, 30].

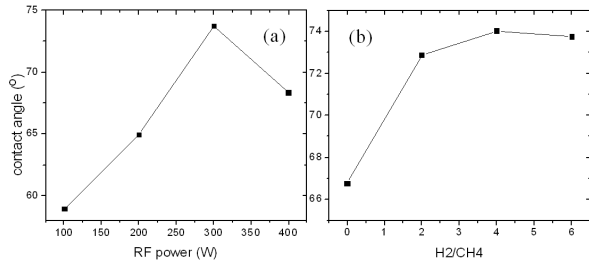


Fig. 9. The dependence of the contact angles on the (a) RF power, (b) gas ratio.

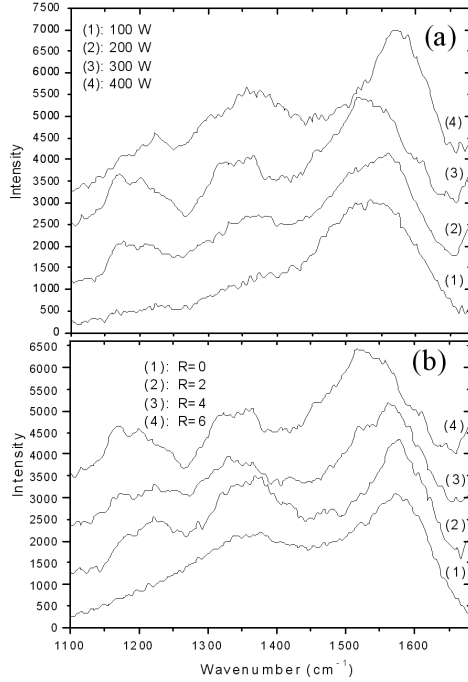


Fig. 10. Raman spectra of deposited DLC films with (a) various RF power, (b) different gas ratio.

TABLE II

$G$  peak position,  $I_D/I_G$  ratio of the Raman spectra with different gas ratios and various RF powers.

$R=H_2/CH_4$	Power of RF [W]	$G$ peak position [nm]	$I_D/I_G$
0	300	1571.56	2.6
2	300	1578.28	1.39
4	300	1562.31	0.76
6	100	1534.45	0.79
6	200	1561.22	0.47
6	300	1517.18	0.23
6	400	1570.67	1.18

As can be seen from Fig. 10a, RF power has no obvious effect on the  $G$  peak position while the intensity ratio decreases from 0.79 to 0.23, up to 300 W; it grows to 1.18 as the power increases to 400 W. This tendency in intensity ratio shows that increasing RF power by more than 300 W transforms the C–C bonds from  $sp^3$  diamond to  $sp^2$  graphite structure. As the hydrogen content increases, the  $G$  peak position shifts to  $1517.18\text{ cm}^{-1}$  and the intensity ratio decreases from 2.6 to 0.23 (Fig. 10b). Therefore introducing more hydrogen content into the plasma has more effects on the quality of DLC films.

#### 4. Conclusion

The properties of DLC thin films deposited by dual-mode PECVD from  $CH_4-H_2$  plasma were investigated. It was found that increase of the RF power to 300 W helps the formation of DLC films with predominant  $sp^3$  phase. The index of refraction grows to 2.63, the roughness initially drops to 0.7764 nm and then increases a little to 0.8248 nm. The more increase of RF power to 400 W reverses this tendency, which is in agreement with the variation of CH,  $C_2$  emission intensity ratios. Increasing the hydrogen content, index of refraction increases continuously to 2.63, the growth rate and roughness go down to 10 nm/min and 0.8248 nm, respectively. This occurs because of more etching of  $sp^2$  rich region by H atoms which stabilizes the carbon  $sp^3$  bonding. As the MW produced plasma has more electrons in energetic tail of the electron energy distribution function, the MW produced plasma considered denser plasma than RF produced plasma. Hence, the growth rate and refractive index rise to 10.8 nm/min and 2.88, respectively as the MW power increases. Therefore, dual frequency technique permits fine-tuning of ion energy and ion flux independently. The water contact angle measurements reveals that as the  $sp^3/sp^2$  fraction of bonding increases and the roughness decreases (films go to show more diamond characteristics), the contact angle grows. The Raman spectroscopy shows that the  $G$  peak position shifts from  $1578.28\text{ cm}^{-1}$  toward  $1517.18\text{ cm}^{-1}$  and intensity ratio decreases from 2.6 to 0.23 by increasing the hydrogen content of the plasma. The RF power only changes the intensity ratio, decreases it from 0.79 to 0.23, up to 300 W, and grows it to 1.18 as the power increases to 400 W.

#### References

- [1] S. Aisenberg, R. Chabot, *J. Appl. Phys.* **42**, 2953 (1971).
- [2] K. Enke, *Thin Solid Films* **80**, 227 (1981).
- [3] J. Zelez, *J. Vac. Sci. Technol. A, Vac. Surf. Films* **1**, 305 (1983).
- [4] *Handbook of Industrial Diamonds and Diamond Films*, Eds. M.A. Prelas, G. Popovici, L.K. Bigelov, Marcel Dekker, New York 1997, pp. 147–192, 227–253, 1023–1147.

- [5] K. Wang, H. Liang, J. Martin, T. Le Mogne, *Appl. Phys. Lett.* **91**, 051918 (2007).
- [6] R. Paul, S. Das, S. Dalui, R. Gayen, R. Roy, R. Bhar, A. Pal, *J. Phys. D, Appl. Phys.* **41**, 055309 (2008).
- [7] D.L. Pappas, K.L. Saenger, J. Burley, W. Kraków, J.J. Cuomo, T. Gu, R.W. Collins, *J. Appl. Phys.* **71**, 5675 (1992).
- [8] N. Mutsukura, S. Inoue, Y. Machi, *J. Appl. Phys.* **72**, 43 (1992).
- [9] D.R. McKenzie, D. Muller, B.A. Pailthorpe, *Phys. Rev. Lett.* **67**, 773 (1991).
- [10] P. Reinke, W. Jacob, W. Möller, *J. Appl. Phys.* **74**, 1354 (1993).
- [11] J.E. Bourée, C. Godet, B. Drévilion, R. Etemadi, T. Heitz, J. Cernogora, J.L. Fave, *J. Non-Cryst. Solids* **198-200**, 623 (1996).
- [12] M. Weiler, S. Sattel, T. Giessen, K. Jung, H. Erhardt, V.S. Veerasamy, J. Robertson, *Phys. Rev. B* **53**, 1594 (1993).
- [13] S. Goldsmith, E. Çetinörgü, R.L. Boxman, *Thin Solid Films* **517**, 5146 (2009).
- [14] K.L. Bhatia, A.K. Sharma, *J. Non-Cryst. Solids* **61**, 285 (1986).
- [15] D.M. Roessler, *Brit. J. Appl. Phys.* **16**, 1119 (1965).
- [16] D. Adlien, J. Laurikaitien, V. Kopustinskas, Š. Meškinnis, V. Šablinskis, *Mater. Sci. Eng. B* **152**, 91 (2008).
- [17] A. Grill, V. Patel, K.I. Saenger, C. Jahnes, S.A. Cohen, A.G. Schrott, D.C. Edeistein, J.R. Paraszczak, *Mater. Res. Soc. Symp. Proc.* **433**, 155 (1997).
- [18] A. Grill, V. Patel, *Diam. Relat. Mater.* **4**, 62 (1994).
- [19] M. Smietana, J. Szmids, M. Korwin-Pawłowski, N. Miller, A. Elmustafa, *Diam. Relat. Mater.* **17**, 1655 (2008).
- [20] M.R. Wertheimer, M. Moisan, *J. Vac. Sci. Technol. A* **3**, 2643 (1985).
- [21] C. Schwärzler, O. Schnabl, J. Laimer, H. Störi, *Plas. Chem. Plas. Proc.* **16**, 173 (1996).
- [22] J. Angus, C. Hayman, *Science* **241**, 913 (1988).
- [23] L. Xiuqiong, C. Junfang, F. Silie, L. Wei, Z. Maoping, S. Lei, Y. Chunlin, *Plas. Sci. Technol.* **9**, 444 (2007).
- [24] E.C. Rangel, N.C. da Cruz, M.E. Kayama, R.C.C. Rangel, N. Marins, S.F. Durrant, *Plas. Polym.* **9**, 1 (2004).
- [25] H.C. Lin, S.T. Shiue, Y.M. Chou, *Surf. Coat. Technol.* **202**, 5360 (2008).
- [26] R.N. Wenzel, *Ind. Eng. Chem.* **28**, 988 (1936).
- [27] X.B. Yan, T. Xu, S.S. Yue, H.W. Liu, Q.J. Xue, S.R. Yang, *Diam. Relat. Mater.* **14**, 1342 (2005).
- [28] E.F. Hare, E.G. Shafrin, W.A. Zisman, *J. Phys. Chem.* **58**, 236 (1954).
- [29] P. Ha, D. McKenzie, M. Bilek, S. Kwok, P. Chu, B. Tay, *Surf. Coat. Technol.* **201**, 6734 (2007).
- [30] B. Druz, I. Zaritskiy, Y. Yevtukhov, A. Konchits, M. Valakh, B. Shanina, S. Kolesnik, I. Yanchuk, Y. Gromovoy, *Diam. Relat. Mater.* **13**, 1592 (2004).